

Multiyear Arctic Sea Ice Classification Using OSCAT and QuikSCAT

David B. Lindell, *Student Member, IEEE*, and David G. Long, *Fellow, IEEE*

Abstract—Arctic sea ice can be classified as first-year (FY) or multiyear (MY) based on data collected by satellite microwave scatterometers. The Oceansat-2 Ku-band Scatterometer (OSCAT) was operational from 2009 to 2014 and is here used to classify ice as FY or MY during these years. Due to similarities in backscatter measurements from sea ice and open water, a NASA Team ice concentration product derived from passive microwave brightness temperatures is used to restrict the classification area to within the sea ice extent. Classification of FY and MY ice is completed with OSCAT by applying a temporally adjusted threshold on backscatter values. The classification method is also applied to the Quick Scatterometer (QuikSCAT) data set, and ice age classifications are processed using QuikSCAT for 1999–2009. The combined QuikSCAT and OSCAT classifications represent a 15-year record, which extends from 1999 to 2014. The classifications show a decrease in MY ice, while the total area of the ice cover remains consistent throughout winter seasons over the time series.

Index Terms—Ice classification, multiyear (MY) ice, scatterometry, sea ice.

I. INTRODUCTION

ARCTIC sea ice can be broadly classified as first-year (FY) or multiyear (MY) based on reported backscatter values from spaceborne scatterometers [1]–[4]. The Oceansat-2 Ku-band Scatterometer (OSCAT) was launched in 2009 by the Indian Space Research Organization (ISRO) and is similar to NASA's Quick Scatterometer (QuikSCAT). Similarities between OSCAT and QuikSCAT motivate the use of OSCAT to extend a record of FY and MY Arctic sea ice classifications completed by Swan and Long [5] (hereafter SL) using QuikSCAT. The SL QuikSCAT sea ice age record [5] extends from 2002 to 2009 and is concluded by the failure of the spin mechanism of the QuikSCAT sensor in 2009. OSCAT is here used with a modified ice classification algorithm based on the one created by SL. The QuikSCAT classifications are reprocessed using the modified algorithm for 1999–2009, and OSCAT is used to extend this record through 2014.

The differing physical properties of FY and MY ice, including surface roughness, brine content, and ice thickness, contribute to observed differences in backscatter [6], [7]. FY ice,

which persists through the melt season, undergoes changes in ice salinity, surface roughness, and porosity and becomes MY ice in the subsequent winter season. The physical differences between FY and MY ice result in differences in backscatter at microwave frequencies and enable broad classification of ice age as FY or MY from scatterometer backscatter observations [5].

Near the sea ice edge, the area of ice cover can become fragmented by the incursion of ocean waves and swells. Such areas are part of the marginal ice zone (MIZ) [8]. Unfortunately, backscatter measurements from areas of the MIZ and from open water can appear similar to backscatter from MY sea ice. Ice classification using microwave scatterometers is restricted to the area of solid ice, in order to avoid misclassification of regions in the MIZ and areas of open water. The SL algorithm classifies FY and MY Arctic sea ice for a given day by generating a high-resolution (4.45 by 4.45 km/pixel) image of the Ku-band radar backscatter coefficient (σ^0) using the scatterometer image reconstruction (SIR) algorithm [9], [10], identifying the sea ice extent, and applying a threshold on backscatter values in the high-resolution image to classify FY and MY ice within the sea ice extent [5]. After the initial classifications are completed using the SL algorithm, transient areas of classified MY ice appear near the ice edge in some regions. Where true MY ice persists until a melt, these areas of classified MY ice near the ice edge appear and disappear over the course of a few days. Such transient areas appear to be misclassifications caused by high backscatter from the MIZ and are suppressed by applying a correction algorithm to the initial classifications.

In the QuikSCAT ice classifications completed by SL, a threshold on reported brightness temperatures from Advanced Microwave Scanning Radiometer - Earth Observing System (AMSR-E) was used to determine the sea ice extent. The SL record began in 2002 when AMSR-E became operational. Unfortunately, the AMSR-E sensor stopped producing global brightness temperature images in 2011; hence, the same methodology cannot be used to identify the sea ice extent and enable classification with OSCAT, which was operational until 2014. Instead, a threshold on a NASA Team ice concentration product produced with Special Sensor Microwave/Imager (SSM/I) and Special Sensor Microwave Imager/Sounder (SSMIS) is used to identify the sea ice extent [11]. Using the NASA Team ice concentrations, ice classifications are reprocessed for QuikSCAT from 1999 to 2009, and OSCAT is used to extend these classifications through 2014.

This paper describes the ice classification process using OSCAT and QuikSCAT and is organized as follows: Section II gives a background; Section III provides sensor information;

Manuscript received November 7, 2014; revised March 26, 2015 and May 26, 2015; accepted June 28, 2015.

The authors are with the Microwave Earth Remote Sensing Laboratory, Brigham Young University, Provo, UT 84602 USA (e-mail: long@byu.edu).

Color versions of one or more of the figures in this paper are available online at <http://ieeexplore.ieee.org>.

Digital Object Identifier 10.1109/TGRS.2015.2452215

Section IV describes the ice classification process with OSCAT and QuikSCAT; Section V details the MIZ correction algorithm; Section VI provides results, and Section VII concludes.

II. BACKGROUND

Satellite microwave scatterometers are sensors that measure the normalized radar backscatter coefficient (σ^0) of the surface of the earth. High-resolution (4.45 by 4.45 km/pixel) images of σ^0 have been produced using the SIR algorithm on data from OSCAT and QuikSCAT [10], [12]. An analysis of measured σ^0 values over a region can provide information about certain geophysical phenomena, including vector winds over the oceans, soil moisture content, and sea ice age and extent [5], [13]–[15]. The differing backscatter characteristics of FY and MY ice [5] enable areas of FY and MY ice to be identified in high-resolution σ^0 images of the Arctic produced with OSCAT or QuikSCAT. Such images provide a starting point for the SL ice age classification algorithm.

SL identify ice extent to restrict the area of ice classification by applying a threshold on reported brightness temperatures from AMSR-E. A 220-K threshold was found to approximate a 40% ice concentration threshold for the NASA Team ice concentration product [5]. Areas with brightness temperatures lower than 220 K are not classified since they represent areas that may not be solid ice.

The SL QuikSCAT classifications are processed using a temporally adapted threshold, fitted each day, on backscatter values. The backscatter signatures of MY and FY ice are indistinguishable during the summer melt; hence, classifications are only processed from day of year (DOY) 284 to 365 and from DOY 1 to 134 (October 11 to May 14). FY ice, which persists through the summer melt and develops a MY ice backscatter signature, is classified as MY ice beginning on DOY 284.

The classification threshold is determined from an average of yearly σ^0 time series histograms of backscatter values from QuikSCAT for 2002 to 2009. The consistent calibration of QuikSCAT throughout its mission lifetime enables a multiyear average to be directly applied. The histogram of measured backscatter values from Arctic sea ice shows that the values tend to be clustered around a low value for FY ice and a high value for MY ice, with a minimum in the histogram between these two peaks. A fifth-degree polynomial is fitted to the σ^0 data each day to identify the minimum, which then serves as a σ^0 threshold to separate FY ice from MY ice. The classification results are relatively insensitive to the threshold chosen; hence, the precise order of the polynomial is not important. A fifth-degree polynomial is selected because it provides a good fit to the data, while also smoothing variations in the threshold caused by weather, instrument calibration changes, or other phenomena.

After the classification threshold is found, SL classify MY ice during the specified winter days. Pixels in the high-resolution backscatter images with σ^0 values above the threshold are classified as MY ice, while those below the threshold are classified as FY ice.

This paper describes how the SL algorithm is adapted to OSCAT and how the QuikSCAT classifications are reprocessed

using the modified algorithm. Several changes are made to the SL algorithm to complete the OSCAT classifications and the QuikSCAT reprocessing. The NASA Team ice concentration product is chosen to replace AMSR-E because NASA Team ice concentrations are available for the entire extent of the QuikSCAT and OSCAT records (while AMSR-E is not). The QuikSCAT classification threshold uses an average of time series histograms from 1999 to 2009, instead of from 2002 to 2009 as used by SL. The OSCAT classification threshold is derived for each year separately because of OSCAT calibration issues, which result in shifted σ^0 values between years. After classifications are completed by applying the classification threshold, a correction algorithm is applied to reduce spurious classifications, which appear to be caused by high backscatter from the MIZ. These changes to the SL algorithm enable the creation of a consistent 15-year record, which incorporates data from both OSCAT and QuikSCAT.

III. SENSOR INFORMATION

The consistency of the Arctic ice age classification data record is related to the similarity of the OSCAT and QuikSCAT sensors. A comparative summary of OSCAT and QuikSCAT is found in Table I. The sensors have similar features, including antenna dimension, frequency, polarization, and orbital characteristics.

Both OSCAT and QuikSCAT operate at Ku-band using a 1-m dual-feed parabolic antenna with a horizontally polarized (HH) inner beam and a vertically polarized (VV) outer beam. Backscatter from VV is used in this study for ice classification, and the VV incidence angles vary slightly between the two sensors. For QuikSCAT, the VV incidence angle is a constant 54°, and for OSCAT, it is 57°. The difference in incidence angle is particularly relevant to ice classification because σ^0 is partially dependent on incidence angle, and a threshold on σ^0 is used to distinguish between FY and MY ice. The relationship between σ^0 and incidence angle can be linearly approximated with σ^0 decreasing as the incidence angle increases. The difference in incidence angle between OSCAT and QuikSCAT and its effect on backscatter is relevant to selecting a consistent classification threshold on σ^0 .

The scatterometers share a similar sun-synchronous near-polar orbit with similar orbital inclinations of 98.6° and 98.28° for QuikSCAT and OSCAT, respectively. QuikSCAT operates at a slightly greater orbital altitude of 803 km compared to OSCAT's 720 km, but the coverage patterns of the sensors are similar enough that Arctic σ^0 images used for classification can be created at the same temporal resolution. The similarities between the OSCAT and QuikSCAT sensors motivate the use of OSCAT to continue the classification data record in the absence of QuikSCAT data.

IV. ICE CLASSIFICATION

In the modified SL algorithm, the NASA Team ice concentrations are adapted as a replacement for AMSR-E in defining the ice extent to enable classification with QuikSCAT and OSCAT. The use of one ice extent product across the entire QuikSCAT/OSCAT classification record improves the consistency of the

TABLE I
CHARACTERISTICS OF QUIKSCAT AND OSCAT [20]

Parameter	QuikSCAT		OSCAT	
Organization	National Aeronautics and Space Administration (NASA)		Indian Space Research Organization (ISRO)	
Antenna Type	1 m dual-feed parabolic		1 m dual-feed parabolic	
Frequency	13.402 GHz		13.515 GHz	
Orbital Period	101 min (14.25 orbits/day)		99.31 min (14.5 orbits/day)	
Orbital Inclination	98.6°		98.28°	
Equator Crossing	6 A.M/6 P.M.		12 A.M/12 P.M.	
Satellite Altitude	803 km at equator		720 km at equator	
Scan Rate	18 rpm		20.5 rpm	
PRF (per beam)	92.5 Hz		96.5 Hz	
Start Date	June 19, 1999		Sept. 23, 2009	
End Date	Nov. 23, 2009		Feb. 20, 2014	
SIR Image Resolution	4.45- by 4.45-km/pixel		4.45- by 4.45-km/pixel	
	Inner Beam	Outer Beam	Inner Beam	Outer Beam
Polarization	HH	VV	HH	VV
Incidence Angle	46°	54°	49°	57°
Slant Range	1100 km	1245 km	1031 km	1208 km
Swath Width	1400 km	1800 km	1400 km	1836 km
One-way Beamwidth (Az x El)	1.8° x 1.6°	1.7° x 1.4°	1.47° x 1.62°	1.39° x 1.72°

record. Differences between the OSCAT and QuikSCAT sensors are analyzed in order to identify potential sources of inconsistency, and classification thresholds for processing ice classifications with OSCAT and QuikSCAT are also determined.

A. NASA Team Ice Extent

In the first step of the modified SL algorithm, areas of sea ice in high-resolution images of σ^0 over the Arctic are isolated using a NASA Team ice concentration product [11], [16]. The NASA Team product was selected because of its availability and the relative insensitivity of the classification results to the ice extent used. To isolate the sea ice extent, a 40% threshold is applied to NASA Team ice concentration values. The relative insensitivity of classification results to the ice extent motivates the subjective choice of a 40% threshold for consistency with the ice extent used by SL and because of demonstrated use in other ice classification studies [5], [17]. Isolating the area of the sea ice extent targets the classification algorithm to the relevant area of Arctic sea ice.

B. OSCAT Incidence Angle Considerations

Continuing the ice classification data record using data from OSCAT requires dealing with the disparity in incidence angles between QuikSCAT and OSCAT. Fortunately, although the reported σ^0 values from QuikSCAT and OSCAT differ because of the unequal incidence angles, a corrective factor for σ^0 is unnecessary. To determine the separation line between MY and FY ice, a separate histogram series of daily σ^0 values is produced for each year. Borders are placed subjectively to roughly isolate the area of the minimum bin count, then minimum points within the borders are identified, and a MY ice threshold curve is fitted to these points. The resulting threshold effectively ignores any constant shift in σ^0 values because it is calculated relative to the distribution of σ^0 values in the annual histogram. The MY ice threshold thus self-adjusts to the

slightly lower σ^0 values of the OSCAT data, and this alleviates the need for an explicit incidence angle correction factor.

C. Ice Classification Thresholding

After the area of the sea ice extent is identified using the NASA Team ice concentration product, ice within the extent is classified with OSCAT or QuikSCAT. Classifying ice age for OSCAT requires certain modifications to the SL classification algorithm. While a classification threshold is determined for QuikSCAT using a multiyear average of time series backscatter histograms, calibration inconsistencies with OSCAT across the instrument lifetime motivate the adoption of a piecewise threshold calculated independently for each year.

Unfortunately, the original OSCAT σ^0 data set demonstrates small jumps and shifts in reported σ^0 values that appear to be caused by noise and power calibration fluctuations [18]. These shifts appear in a daily series of histograms in Figs. 1 and 2. Some years have consistently higher or lower σ^0 values, and intra-annual variability is particularly apparent in the winter of 2009/2010, where σ^0 values for several days' data jump up and down throughout the year.

The jumps in reported σ^0 that occur during the winter of 2009/2010 require that a correction be applied to the data. For this purpose, the 2009/2010 series of daily histograms is reprocessed using an algorithm that identifies areas of shifted σ^0 values, determines the magnitude of the shift, and applies a correction. The correction is intended to align the data and eliminate shifts in σ^0 values. Uncorrected and corrected versions of the 2009/2010 annual histogram are shown in Fig. 2. With the removal of the shifts, the corrected version shows significantly improved continuity.

Although SL use a multiyear average of the QuikSCAT σ^0 time series histograms to calculate a MY ice threshold, averaging OSCAT data across years yields an undesirable threshold curve because of the instrument anomalies. Instead of using the multiyear average for OSCAT, a piecewise threshold model is determined for each year separately. Bounds are set subjectively

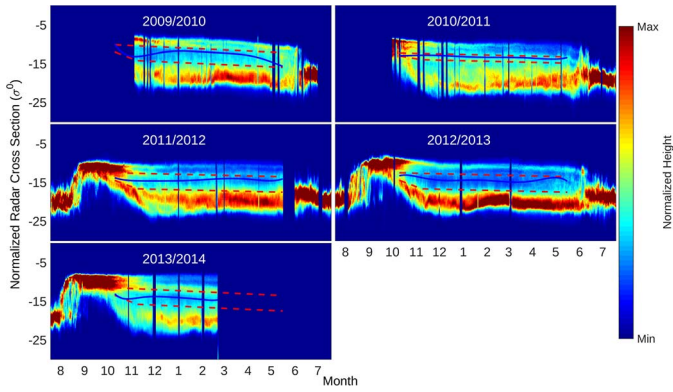


Fig. 1. Time series of OSCAT daily σ^0 histograms for the winter seasons from 2009 to 2014. A blue curve is fitted to minimum points and used as a threshold for FY and MY ice classification. The red dashed lines are subjective bounds used to constrain the threshold to the area between peak distributions corresponding to FY and MY ice.

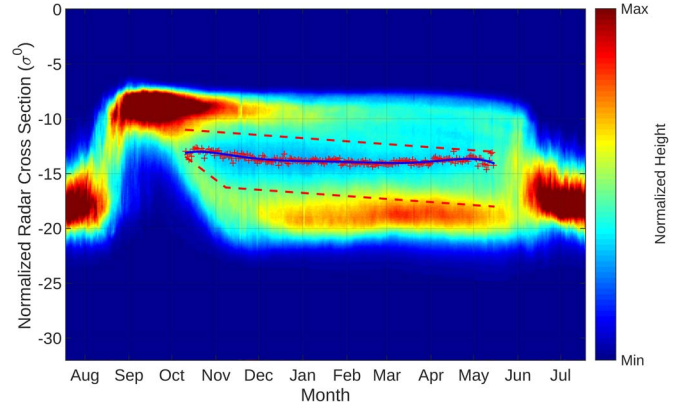


Fig. 3. Average time series of QuikSCAT daily σ^0 histograms. An average histogram of backscatter values for each DOY is created by averaging daily backscatter histograms from 1999 to 2009. The resulting averaged daily histograms are concatenated into this time series image. A blue curve is fitted to minimum points and used as a threshold for FY and MY ice classification. The red dashed lines are subjective bounds used to constrain the threshold to the area between peak distributions corresponding to FY and MY ice.

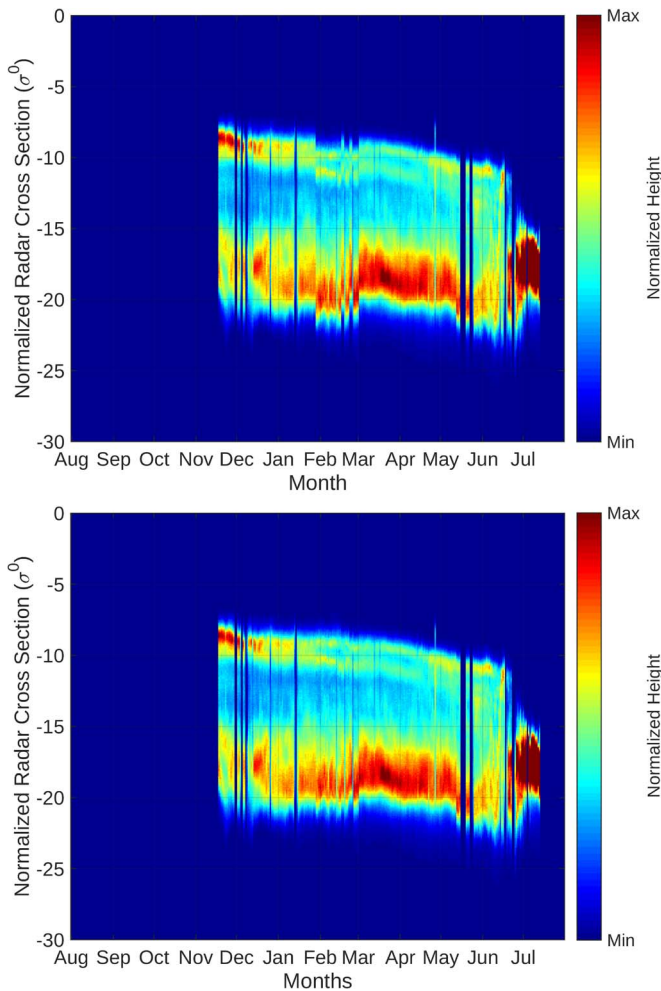


Fig. 2. Uncorrected OSCAT data (upper) and corrected data (lower) for the winter of 2009/2010 shown in a collection of daily histograms.

for each histogram of winter σ^0 values (DOY 284 to DOY 134) by attempting to isolate the area of minimum bin counts that persists for most of the winter. The minimum points between the bounds are then identified, and a fifth-degree polynomial is fitted to these minimum points. Days that do not occur between

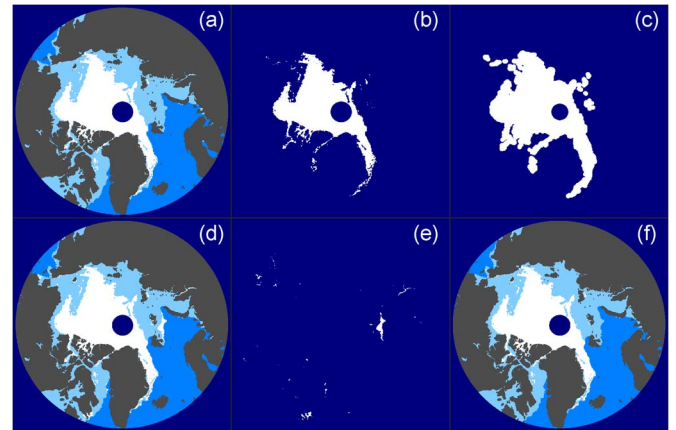


Fig. 4. Image series showing the application of the MIZ correction algorithm for DOY 1–2, 2001. MY ice is shown in white with FY ice in pale blue. Image A shows classifications from DOY 1, 2001, after the MIZ correction algorithm has been applied. A mask of the area of MY ice from image a is created (image b) and dilated (image c). The initial classifications for DOY 2, 2001 (image d) are compared with the dilated area of MY ice from the previous day (image c). Areas of initially classified MY ice, which fall outside of the dilated mask (image e), are removed from the initial classifications. The corrected classifications for DOY 2, 2001, are shown in image f.

DOY 284 and DOY 134 are considered to be part of the summer melt, and ice is not classified during this period. This classification scheme results in a piecewise function, which is used as a MY ice threshold. MY ice threshold curves for each year are shown in Fig. 1. The threshold curves vary from about -12 dB to -15 dB and the bounds fluctuate between -10 dB and -17 dB, depending on the year. The variation in the curves and bounds is due in part to the interannual shifts in reported σ^0 values, which skew the data sets. Application of these thresholds to OSCAT produces a consistent data set for the years 2009–2014.

QuikSCAT ice age classifications are reprocessed using an average time series of QuikSCAT daily σ^0 histograms to determine the classification threshold. To produce the average histogram time series, an average histogram for each DOY is computed using daily σ^0 histograms from 1999 to 2009. The

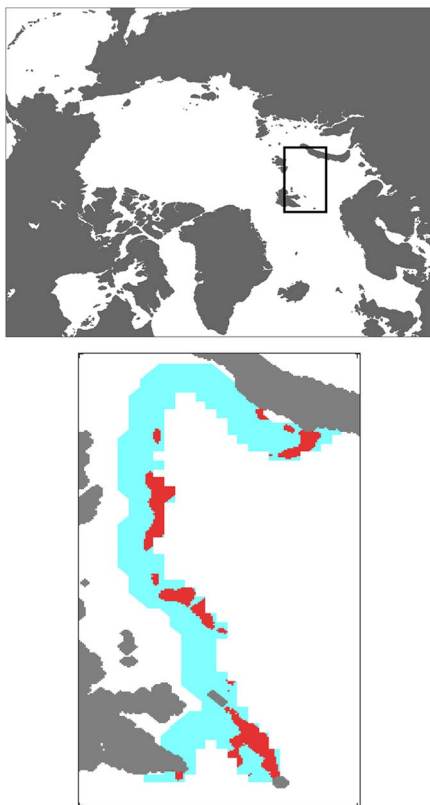


Fig. 5. Map delineating the study region south and east of the island of Svalbard (upper) and a closer perspective (lower) showing the effect of the MIZ correction algorithm. Blue pixels in the right image represent FY ice within 90 km of the ice edge. Red pixels represent ice which was reclassified as FY from MY by the MIZ correction algorithm. White pixels represent ice or open ocean outside the MIZ study region.

resulting average daily histograms are arranged in a time series and reveal the average temporal progression of backscatter distributions throughout the year. The threshold is determined by fitting a fifth-degree polynomial to bin count minima in the average histogram series between peak distributions representing FY and MY ice. The average time series histogram, minimum bin points, and classification threshold are shown in Fig. 3. The resulting classifications extend the previous SL ice age classifications backward for the years 1999–2002. These years were not classified by SL because AMSR-E had not yet become operational. The full QuikSCAT data set extends from 1999 to 2009.

V. MIZ CORRECTION ALGORITHM

The MIZ is characterized by fragmented ice floes near the ice edge, which are broken up by incoming waves. This slurry of ice near the ice edge is a transition zone between a thicker continuous ice sheet and the ocean. The rough surface properties of the MIZ can result in high radar backscatter, which exceeds the classification threshold used to distinguish between FY and MY ice. When the classification threshold is applied, certain areas of the MIZ can be erroneously classified as MY ice.

MIZ ice, which is incorrectly classified as MY ice, must be distinguished from true areas of MY ice that occur near the ice edge. One such area of MY ice near the ice edge is off the

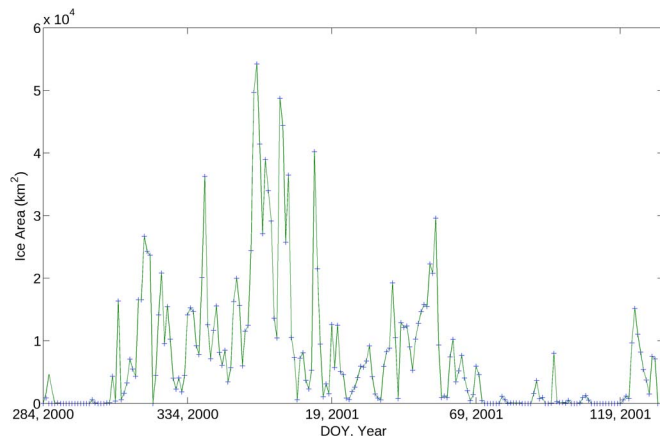


Fig. 6. Plot of classified MY ice near the ice edge south and east of the island of Svalbard for the winter of 2000/2001. The solid line indicates the total area of classified MY in the area near the ice edge before the correction algorithm is applied. The cross markers indicate the area of classified MY ice, which was reclassified as FY ice. Data points from the plots are almost always the same because nearly all of the classified MY ice is reclassified as FY ice.

east coast of Greenland. In this region, a significant part of the main body of Arctic MY ice advects south and is ejected into the Atlantic ocean. A correction algorithm is described, which distinguishes between MY ice and misclassified areas of the MIZ, and is sensitive to true areas of MY ice near the ice edge.

A. Correcting MY Ice Misclassifications

Areas in the MIZ where FY ice is initially misclassified as MY ice can be distinguished from other areas of MY ice based on the temporal transience of the backscatter from the MIZ. High backscatter values throughout the MIZ typically persist for only one to two days, whereas backscatter from MY ice areas remains high as long as melt does not occur. By observing classification patterns over multiple days, misclassification errors can be reduced. The goal of the correction algorithm is to reduce the misclassified MY ice.

The algorithm to mitigate MIZ errors in ice classification uses images of the Arctic where FY and MY ice have already been initially classified. All pixels classified as MY ice are identified and used to create a mask. The mask is then dilated and compared to the area of classified MY ice in the image for the subsequent day. All MY ice which appears outside of the dilated mask is reclassified as FY ice. The process then repeats with a new mask of MY ice being created from the newly adjusted classification image. Fig. 4 provides a visual example of the steps of the MIZ correction process. The figure shows that areas of misclassified MY ice in the outside of the derived MY ice mask are reclassified as FY ice.

B. Correction Algorithm Performance

The performance of the correction algorithm is evaluated using a quantitative measure of the amount of ice that it reclassifies as FY. An area south and east of the island of Svalbard, where misclassified MY ice appears frequently, and another area near the east side of Greenland are analyzed.

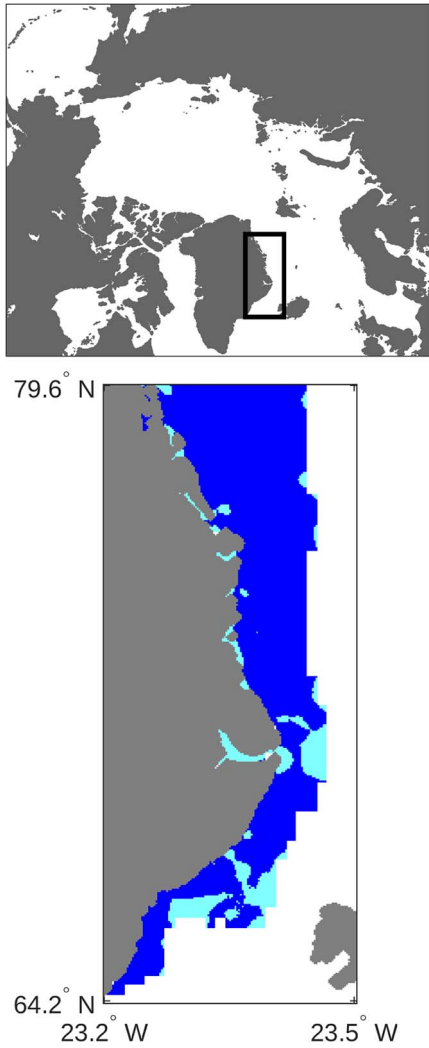


Fig. 7. Map delineating the study region on the east coast of Greenland (upper) and a closer perspective (lower) showing ice classifications after applying the MIZ correction algorithm. White pixels in the right image represent ocean areas outside the MIZ. Dark blue and turquoise pixels represent areas classified as MY and FY ice, respectively. In this case, the initial classifications were not changed by the correction algorithm.

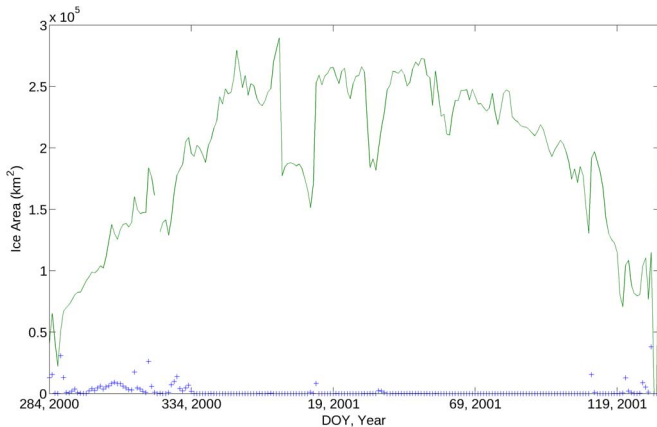


Fig. 8. Plot of classified MY ice near the east coast of Greenland for 2000–2001. The solid line indicates the total area of classified MY in the area near the ice edge before the correction algorithm is applied. The cross markers indicate the area of classified MY ice which was reclassified as FY ice. Days with missing data produce gaps in the plot.

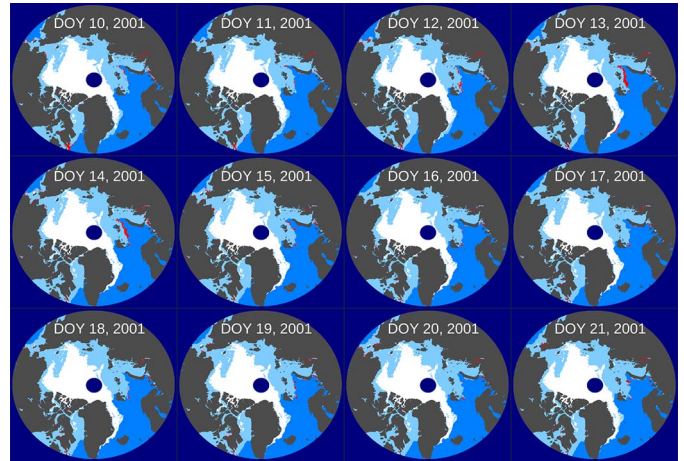


Fig. 9. Time series of images from DOY 10 to 21, 2001, where the correction has been applied. MY ice is shown in white, FY ice is pale blue, and ocean is medium blue. Areas of initially classified MY ice that have been reclassified as FY ice are shown in red.

The area near the island of Svalbard extends from 72.6° N latitude to 79.2° N latitude and from 19.4° E longitude to 71.26° E longitude. The ice edge typically falls within this area during the winter, and the regions of misclassified MY ice generally appear within 90 km of the ice edge. For each day in which ice is classified, pixels located within 90 km of the ice edge are identified and analyzed. Fig. 5 shows an example image of the area near the ice edge and identifies regions where the ice classification was changed from MY to FY.

Much of the ice initially classified as MY near the ice edge is transient and characteristic of misclassifications caused by the MIZ. Fig. 6 shows a plot of the area of MY ice and the area of reclassified MY ice within the region near the ice edge for the winter of 2000/2001. At the beginning and end of the winter, the area of initially classified MY ice near the ice edge is minimal, although the amount increases during the middle of the winter, varying from around 10 000 to 50 000 km^2 within the study region. The high variability of the levels of initially classified MY ice is not characteristic of true MY ice, which persists until a melt occurs. We postulate that high backscatter from the MIZ has resulted in incorrect initial MY ice classifications. The correction algorithm consistently reclassifies these transient areas of MY ice as FY ice.

Near the east coast of Greenland, some areas of MY ice exist near the ice edge. A study area is defined to explore the effects of the MIZ correction in this area and extends from 64.2° N latitude to 79.6° N latitude and from 23.2° W longitude to 23.5° W longitude. Fig. 7 shows an image of the region and identifies pixels classified as MY and FY ice within the region. Since much of the ice in this area appears to be true MY ice, the MIZ correction algorithm should not typically reclassify any MY ice to FY ice.

The performance of the MIZ correction algorithm is shown for the winter of 2000/2001 in Fig. 8. The area of MY ice near the coast of Greenland increases throughout the winter before decreasing prior to the summer melt. The MIZ correction algorithm reclassifies a minimal amount of MY ice to FY ice. This is consistent with the SL results and is the desired performance

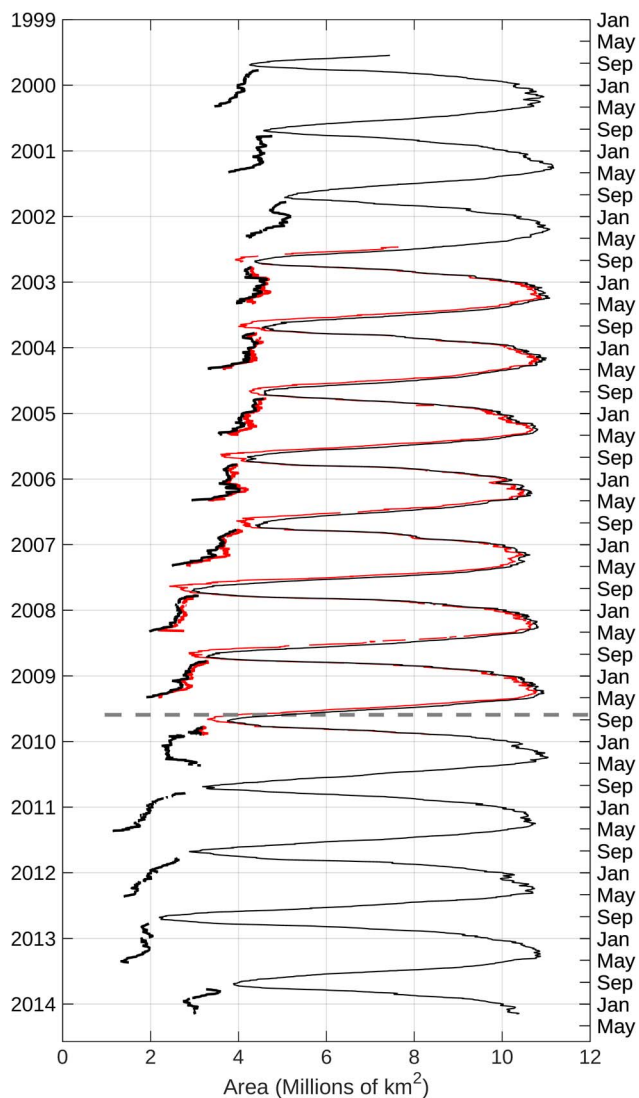


Fig. 10. Plot of total Arctic ice area and MY ice area derived from QuikSCAT and OSCAT. The total area of Arctic ice extent is shown by the thin red and black lines. The thin black line indicates ice extent calculated using the NASA Team ice concentration product. The thin red line indicates the ice extent calculated using the SL method of applying a brightness temperature threshold to data from AMSR-E. Area of MY ice is shown by the thick red and black lines. The thick red line indicates area of MY ice classified using the SL algorithm. The thick black line indicates MY ice classified using QuikSCAT or OSCAT and the modified SL algorithm. MY ice for years above the dashed gray line is classified with QuikSCAT, while for years below it is classified with OSCAT.

because the initial classifications of MY ice near the east coast of Greenland appear to correctly identify areas of true MY ice.

The MIZ correction algorithm appears to correctly identify and correct areas of erroneously classified MY ice near the ice edge. A time series of corrections applied in 2001 is shown in Fig. 9. Throughout the time series, areas of MY ice, which have been reclassified as FY ice, are shown in red. The time series demonstrates that the algorithm can effectively reclassify ice in multiple areas near the ice edge, while leaving consistent areas of true MY ice unperturbed. The correction algorithm is applied to the initial QuikSCAT and OSCAT ice classifications, in order to remove misclassified MY ice.

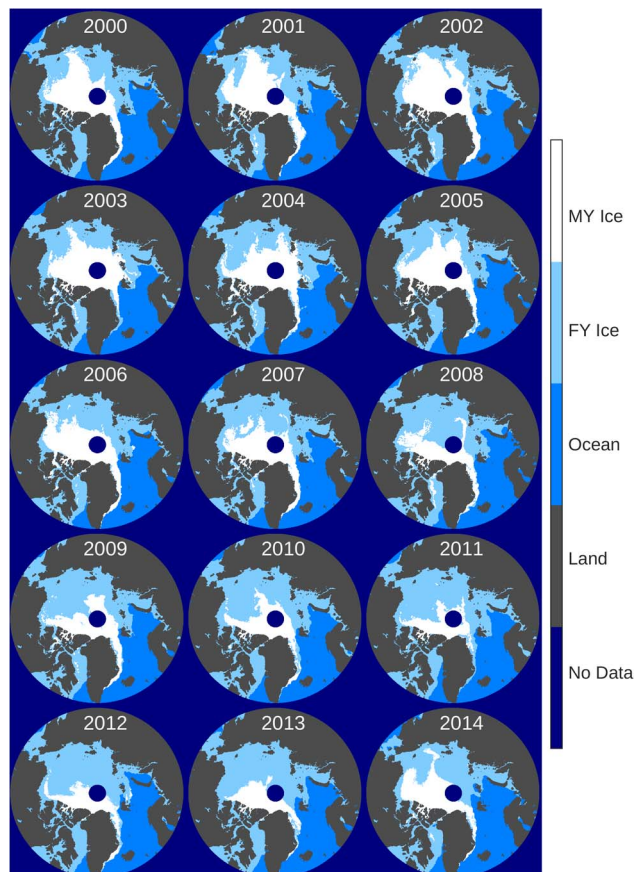


Fig. 11. Maps of FY and MY ice, land, and ocean for DOY 45 from 2000 to 2014. The maps from 2000 to 2009 use data from QuikSCAT, and maps from 2010 to 2014 use data from OSCAT.

VI. TIME SERIES RESULTS: 1999–2014

Ice classifications completed using OSCAT and QuikSCAT result in a nearly continuous record from 1999 to 2014 that can be analyzed to determine trends in Arctic ice levels. Plots of MY ice area and ice extent area throughout the time series are shown in Fig. 10. MY ice levels are derived from the ice classifications created from the MY ice threshold curves and data from QuikSCAT and OSCAT. The total ice area is calculated by applying a 40% threshold to the NASA Team ice concentration product to determine ice extent. The area of the pole hole is a no-data region and is not added to the ice extent or MY ice areas. Jumps or increases in the area of MY ice during winter seasons throughout the time series are due to areas near the ice edge, which demonstrate high backscatter for several days before decreasing. In these cases, the ice is classified as MY despite the correction algorithm because of the persistence of the high backscatter values. Larger shifts in MY ice area occur at a few instances in the time series, when such areas of high backscatter appear near the ice edge close to the east coast of Greenland or near the Davis Strait.

The greatest area of MY ice appears to occur in 2003, and the area of MY ice declines in the following years, reaching a low in 2013. For winter seasons during the time series (from October to May), the average change in MY ice area is a decrease of approximately 846 000 km². The greatest decrease in

winter-averaged MY ice area is roughly 853 000 km² between the winters of 2006/2007 and 2007/2008; the greatest increase is roughly 1.24 million km² between the winters of 2012/2013 and 2013/2014.

General trends in FY and MY ice area are shown in Fig. 11, which shows classification images from DOY 45 for each year of the time series. The decrease in MY ice appears to be influenced by the advection of ice into the Atlantic Ocean occurring on the east coast of Greenland and through the Davis Strait. In 2014, the MY ice area appears to recover somewhat and is comparable to levels observed in 2005 or 2006. The total area of the ice extent is seasonally dependent, although the peak extent area in winters throughout the time series is relatively consistent (around 11 million km²). The lowest ice extent area is observed in the summer of 2012, although in 2013 the summer ice extent increases and is also comparable to levels observed in 2005 or 2006. Overall, the results indicate a general decline in the area of MY ice with a possible recovery of ice area in 2014.

The QuikSCAT classifications reprocessed with the modified algorithm demonstrate similar results to those processed by SL, although slight differences in reported ice extent area and MY ice area can be observed. As shown in Fig. 10, the ice extent calculated with a threshold on AMSR-E brightness temperature images corresponds well to the 40% ice concentration threshold on the NASA Team ice product. The NASA Team-derived ice extent is an average of 164 800 km² greater than the AMSR-E extent during winter days, in which ice age is classified from 2002 to 2009.

The MY ice area of the reprocessed QuikSCAT classifications is an average of 127 000 km² lower than the SL classifications. The lower MY ice area of the reprocessed classifications is partly due to the MIZ correction algorithm, which removes some erroneously classified areas of MY ice that are present in the SL classifications. Before the correction algorithm is applied, the average area of MY ice in the reprocessed classifications is only 29 400 km² lower than the SL classifications. The results from the reprocessed data thus correspond well to the previous SL results.

VII. CONCLUSION

Ice age classifications processed with OSCAT data extend the QuikSCAT classification record, resulting in a 15-year record that extends from 1999 to 2014. Classifications completed with QuikSCAT agree well with classifications previously completed by SL and demonstrate a marked decrease in the amount of Arctic MY ice across the data set. The classification data are distributed publicly as part of the NASA Scatterometer Climate Record Pathfinder project (<http://www.scp.byu.edu>).

Due to the failure of OSCAT in 2014, future work to extend the ice classification data set will require a different sensor. There are currently no fully operational Ku-band sensors, which could be used; however, the C-band Advanced Scatterometer (ASCAT)-A and -B sensors (launched by the European Space Agency in 2006 and 2012) are currently operational. To adapt the ice classification algorithm to the ASCAT sensors, the differences in sensitivity to FY and MY

ice at C-band compared to Ku-band would need to be addressed. The longer wavelength of the ASCAT sensors compared to QuikSCAT or OSCAT results in decreased sensitivity to volume scattering from porous MY ice and increased responsiveness to backscatter from the MIZ [19]. The decreased sensitivity to differences between FY and MY ice at C-band compared to Ku-band might be improved by combining passive microwave data with the C-band scatterometer observations in an adapted classification algorithm. Additional steps to mitigate ice misclassifications in the MIZ might also be required because of the higher sensitivity to MIZ ice at C-band compared to Ku-band.

Although it is not fully operational, QuikSCAT could also still be used to classify ice age over the Arctic. Due to the failure of its spin mechanism in 2009, QuikSCAT is restricted to a single azimuthal scan angle, resulting in a significant decrease in spatial coverage. Despite this, σ^0 images of the Arctic could possibly be produced with QuikSCAT at decreased temporal resolution and used for classification purposes for years after 2009.

REFERENCES

- [1] N. Walker, K. Partington, M. Van Woert, and T. Street, "Arctic sea ice type and concentration mapping using passive and active microwave sensors," *IEEE Trans. Geosci. Remote Sens.*, vol. 44, no. 12, pp. 3574–3584, Dec. 2006.
- [2] R. G. Onstott, "SAR and scatterometer signatures of sea ice," in *Microwave Remote Sensing of Sea Ice*. Washington D.C., USA: Amer. Geophys. Union, 1992.
- [3] M. Hallikainen and D. P. Winebrenner, "The physical basis for sea ice remote sensing," in *Microwave Remote Sensing of Sea Ice*. Washington D.C., USA: Amer. Geophys. Union, 1992.
- [4] G. Belchansky and D. Douglas, "Classification methods for monitoring Arctic sea ice using OKEAN passive/active two-channel microwave data," *Remote Sens. Environ.*, vol. 73, no. 3, pp. 307–322, Sep. 2000.
- [5] A. Swan and D. Long, "Multi-year Arctic sea ice classification using QuikSCAT," *IEEE Trans. Geosci. Remote Sens.*, vol. 50, no. 9, pp. 3317–3326, Sep. 2012.
- [6] W. Tucker, D. Perovich, A. Gow, W. Weeks, and M. Drinkwater, "Physical properties of sea ice relevant to remote sensing," in *Microwave Remote Sensing of Sea Ice*. Washington D.C., USA: Amer. Geophys. Union, 1992.
- [7] W. Tucker *et al.*, "Microwave and physical properties of sea ice in the winter marginal ice zone," *J. Geophys. Res.: Oceans*, vol. 96, no. C3, pp. 4573–4587, 1991. [Online]. Available: <http://dx.doi.org/10.1029/90JC02269>
- [8] J. Haarpaintner, R. Tonboe, D. Long, and M. Van Woert, "Automatic detection and validity of the sea-ice edge: An application of enhanced-resolution QuikScat/SeaWinds data," *IEEE Trans. Geosci. Remote Sens.*, vol. 42, no. 7, pp. 1433–1443, Jul. 2004.
- [9] D. Early and D. Long, "Image reconstruction and enhanced resolution imaging from irregular samples," *IEEE Trans. Geosci. Remote Sens.*, vol. 39, no. 2, pp. 291–302, Feb. 2001.
- [10] M. Spencer, C. Wu, and D. Long, "Improved resolution backscatter measurements with the SeaWinds pencil-beam scatterometer," *IEEE Trans. Geosci. Remote Sens.*, vol. 38, no. 1, pp. 89–104, Jan. 2000.
- [11] D. Cavalieri, C. Parkinson, P. Gloersen, and H. Zwally, "Sea ice concentrations from Nimbus-7 SMMR and DMSP SSM/I-SSMIS passive microwave data. [Subset 1999–2014]. NASA Nat. Snow Ice Data Center Distrib. Active Archive Center, Boulder, CO, USA, 1996.
- [12] D. Long, P. Hardin, and P. Whiting, "Resolution enhancement of spaceborne scatterometer data," *IEEE Trans. Geosci. Remote Sens.*, vol. 31, no. 3, pp. 700–715, May 1993.
- [13] M. Owen and D. Long, "Simultaneous wind and rain estimation for QuikSCAT at ultra-high resolution," *IEEE Trans. Geosci. Remote Sens.*, vol. 49, no. 6, pp. 1865–1878, Jun. 2011.
- [14] I. Mladenova, V. Lakshmi, J. Walker, D. Long, and R. De Jeu, "An assessment of QuikSCAT Ku-band scatterometer data for soil moisture

sensitivity," *IEEE Geosci. Remote Sens. Lett.*, vol. 6, no. 4, pp. 640–643, Oct. 2009.

- [15] Q. Remund and D. Long, "A decade of QuikSCAT scatterometer sea ice extent data," *IEEE Trans. Geosci. Remote Sens.*, vol. 52, no. 7, pp. 4281–4290, Jul. 2014.
- [16] J. Bradley and D. Long, "Estimation of the OSCAT spatial response function using island targets," *IEEE Trans. Geosci. Remote Sens.*, vol. 52, no. 4, pp. 1924–1934, Apr. 2014.
- [17] D. Cavaliere, "NASA Team Sea Ice Algorithm," Nat. Aeronaut. Space Admin. (NASA), Washington, DC, USA, May 2003. [Online]. Available: <http://nsidc.org/data/docs/daac/nasateam/>
- [18] W. Meier and J. Stroeve, "Comparison of sea-ice extent and ice-edge location estimates from passive microwave and enhanced-resolution scatterometer data," *Ann. Glaciol.*, vol. 48, pp. 65–70, 2008.
- [19] S. Bhowmick, R. Kumar, and A. Kumar, "Cross calibration of the OceanSAT-2 scatterometer with QuikSCAT scatterometer using natural terrestrial targets," *IEEE Trans. Geosci. Remote Sens.*, vol. 52, no. 6, pp. 3393–3398, Jun. 2014.
- [20] M. Rivas, J. Verspeek, A. Verhoef, and A. Stoffelen, "Bayesian sea ice detection with the Advanced Scatterometer ASCAT," *IEEE Trans. Geosci. Remote Sens.*, vol. 50, no. 7, pp. 2649–2657, Jul. 2012.



David B. Lindell (S'13) was born in Fairmont, MN, in 1990. He received the B.S. degree (*summa cum laude*) in electrical engineering from Brigham Young University (BYU), Provo, UT, USA, in 2015. He is currently working toward the M.S. degree in electrical engineering at BYU.

Since April 2014, he has been a Research Assistant with the Microwave Earth Remote Sensing Laboratory at BYU. His research involves various geoscience applications of microwave remote sensing.



David G. Long (S'80–M'82–SM'98–F'09) received the Ph.D. degree in electrical engineering from the University of Southern California, Los Angeles, CA, USA, in 1989.

From 1983 to 1990, he was with NASA's Jet Propulsion Laboratory (JPL), where he developed advanced radar remote sensing systems. While at JPL, he was the Project Engineer on the NASA Scatterometer (NSCAT) Project, which flew from 1996 to 1997. He also managed the SCANSAT Project, the precursor to SeaWinds, which was launched in

1999, 2002, and 2014. He is currently a Professor with the Department of Electrical and Computer Engineering, Brigham Young University, Provo, UT, USA, where he teaches upper division and graduate courses in communications, microwave remote sensing, radar, and signal processing and is the Director of the BYU Center for Remote Sensing. He is the Principal Investigator on several NASA-sponsored research projects in remote sensing. He has over 400 publications in signal processing and radar scatterometry. His research interests include microwave remote sensing, radar theory, space-based sensing, estimation theory, signal processing, and mesoscale atmospheric dynamics.

Dr. Long has received the NASA Certificate and Team Recognition Award several times. He is currently an Associate Editor for the *IEEE GEOSCIENCE AND REMOTE SENSING LETTERS*.